Journal of Engineering Science and Technology
Vol. 12, No. 6 (2017) 1662 - 1676

CFD SIMULATION FOR DEMILITARIZATION OF RDX IN A ROTARY KILN BY THERMAL DECOMPOSITION

SI H. LEE[1], WOO Y. JEONG[1], BAGGIE W. NYANDE[1], JUNG SU PARK[2], IL MOON[3], MIN OH[1,*]

[1]Department of Chemical & Biological Engineering, Hanbat national university, Daejeon, South Korea
[2]Agency for Defense Development, Daejeon, South Korea
[3]Department of Chemical & Biomolecular Engineering, Yeonsei University, Seoul, South Korea
*Corresponding Author: minoh@hanbat.ac.kr

Abstract

Demilitarization requires the recovery and disposal of obsolete ammunition and explosives. Since open burning/detonation of hazardous waste has caused serious environmental and safety problems, thermal decomposition has emerged as one of the most feasible methods. RDX is widely used as a military explosive due to its high melting temperature and detonation power. In this work, the feasible conditions under which explosives can be safely incinerated have been investigated via a rotary kiln simulation. To solve this problem, phase change along with the reactions of RDX has been incisively analyzed. A global reaction mechanism consisting of condensed phase and gas phase reactions are used in Computational Fluid Dynamics simulation. User Defined Functions in FLUENT is utilized in this study to inculcate the reactions and phase change into the simulation. The results divulge the effect of temperature and the varying amounts of gas produced in the rotary kiln during the thermal decomposition of RDX. The result leads to the prospect of demilitarizing waste explosives to avoid the possibility of detonation.

Keywords: Demilitarization, Thermal decomposition, RDX, CFD simulation, Rotary Kiln.

1. Introduction

Hexahydro-1, 3, 5-trinitro-1, 3, 5-triazine (RDX) a cyclic nitramine characterized by high melting point and enormous energy upon detonation [1], has been continuously used as an industrial explosive and in pristine forms for military

Nomenclatures

$A_{n,RDX}$	Heat transfer area of solid and liquid RDX, m^2
A_j	Collision factor of CPR and GPR, 1/s or m^3/mol·s
$C_{j,i}$	Concentration of reactant, mol/m^3
E_j	Activation energy of CPR and GPR, J/mol
$\vec{g}$	Gravity acceleration, m/s^2
$H_{latent,k}$	Latent heat of solid and liquid RDX, J/mol
$(\Delta H_r)_j$	Heat of reaction of CPR and GPR, J/mol
h_{pq}	Interface enthalpy between phase p and q, J/kg
h_q	Specific enthalpy of phase q, J/kg
h	Heat transfer coefficient by convection, J/m^2·K·s
$\vec{J}_i$	Diffusion flux of species i, kg/ m^2·s
MW_i	Molecular weight of RDX and each species i, kg/mol
$\dot{m}_{pq}$	Mass transfer from phase q to phase p, kg/m^3·s
p_q	Static pressure shared by all phases, Pa
$\vec{Q}_{pq}$	Intensity of heat exchange between phase p and q, J/m^3·s
q^k	Heat rate by heat transfer, J/s
$\vec{q}_q$	Heat flux of phase q, J/m^2·s
R	Ideal gas constant, J/mol·s
$\vec{R}_{pq}$	Interaction force between phase p and q, Pa/m
r_j	Reaction rate of CPR and GPR, mol/m^3·s
Se	Energy source by phase change and reaction, J/m^3·s
$S_{F,q}$	Force source of phase q, Pa/m
Sm	Mass source by phase change and reaction, mol/m^3·s
T_{RDX}^n	Temperature of solid and liquid RDX, K
T_{air}	Temperature of air inside of rotary kiln, K
$V_{reactor}$	Volume of reactor, m^3
$\vec{v}$, $\vec{v}_q$	Velocity of mixture and phase q, m/s
$\vec{v}_{pq}$	Interface velocity between phase p and q, m/s
Y_i	Mass fraction of each species i

Greek Symbols

α_q	Volume fraction of phase q
ρ_q , ρ	Density of phase q and mixture, kg/m^3
$\bar{\bar{\tau}}_q$	Stress-strain tensor of phase q, Pa
$\xi_{j,i}$	The number of Stoichiometry, dimensionless

Abbreviation

CPR	Condensed Phase Reaction
GPRs	Gas Phase Reactions
CFD	Computation Fluid Dynamics
UDF	User Defined Function

applications [2]. In spite of the numerous desired characteristics, RDX has an inevitably high sensitivity to heat and shock which dictates the precision required in its processing and demilitarization. Demilitarization which embodies the various unit operations required in disposing obsolete and unused ammunitions in a safe and an environmentally benign way has become a pressing issue. Quite a limited number of ways exist to achieve this end which includes 1) open burning/detonation 2) biological treatment 3) supercritical oxidation and 4) incineration in rotary kilns [3, 4]. Until recently, open burning/detonation have been the primary means of demilitarization. This low-cost method is out of vogue due to environmental limitations on the concentrations of toxic gases. While biological treatment methods are relatively inexpensive compared with incineration, several questions concerning its applicability in treating RDX and other nitrated energetic compounds still remain unanswered. For instance, failure of lining materials used in biological ponds, a ubiquitous occurrence, results in the contamination of groundwater due to rapid seepage of RDX [5]. The biodegradation of RDX in activated sludge reactors involving the use of both anoxic and aerobic filters is yet to meet anticipated regulatory targets [6]. Considerable efforts have been made toward the study of RDX reactions. These reactions primarily occur in the condensed and gaseous phases. A total of 3 global reactions [7] were used to represent the entire RDX decomposition after analyzing the detailed combustion reaction of 263 [8, 9]. Similar work done delved into the proposed global reactions by Liau [10]. Their studies made mention of liquid decomposition of RDX and also evaporation occurring at 491 K-515 K and 573 K-620 K respectively [8, 11].

Other works [12-14] provide information about the kinetics of RDX reaction through thermal analysis such as DSC and TGA. In this study, we carry out a CFD simulation using FLUENT [15] on a demilitarization facility in Korea, which is currently being operated to deal with small-sized munitions [16]. The facility consists of a rotary kiln, an elution, and a disabling facility. Thermal decomposition of munitions in the rotary kiln is carried out by heating until combustion occurs. Thermal decomposition of RDX involves phase transformation from solid to the gaseous phase through a rather ephemeral liquid phase with a two-stage chemical process involving condensed and gas phase reactions [17-19]. Multiphase reactive flows are quite intricate and pose significant modelling challenges. By using the Eulerian approach in CFD, [20] developed a model for the production of polypropylene in a pilot scale reactor. Jung et al. [21] in their work on the crystallization of RDX relied on the two-phase Eulerian model. Although very rigorous, the multi-fluid Eulerian approach allows for effective handling of complex reactions and interphase phenomena including heat and mass transfer at a relatively cheaper computational cost and is thus adopted in this work. This work aims at investigating the safe operating conditions for the thermal decomposition of RDX in a rotary kiln. Global kinetics and phase change have been introduced into the CFD solver by UDF to

investigate the optimum conditions for the operation of the rotary kiln while avoiding the creation of hotspots and the possibility of detonation.

2. Theoretical Background

Rotary kilns are currently in use for diverse applications ranging from calcination to the incineration of hazardous waste. Regardless of the specific design, rotary kilns generally comprise of preheating, combustion, and cooling zones along their axial length [22]. Thermal decomposition of RDX in a rotary kiln depends on the operating conditions, specifically feed rate, temperature, and flow rates of air. The influence of these parameters is evident in the composition of combustion products. In this study, 1.97 kg of RDX was introduced into the rotary kiln and subjected to heating. There was a phase transition from solid to liquid at a temperature of 478 K (melting point). Evaporation of liquid RDX occurred at an elevated temperature of 507 K. The liquid RDX, which was produced due to melting, reacts in the condensed phase to produce gaseous products alongside phase change to the gas phase. Continual increase in temperature led to thermal decomposition at a temperature of 533 K. The Eulerian multiphase model was used to solve the governing equations for each of the three phases. Phase change and chemical reactions were included through a UDF.

The mass source Sm_q , $Sm_{g,i}$ represents the rate at which gases and liquid are generated through melting, evaporation, and chemical reactions. The energy source (Se_q) encompasses the heat of reaction and the enthalpy associated with the phase transition of RDX. In order to solve these mass sources, the UDF solver requires the temperature of air (T_{air}) and RDX (T_{RDX}) and concentration of gas phase reactant $C_{j,i}$ as illustrated in Fig. 1.

2.1. CFD model

The 3D model of the rotary kiln was developed using the exact dimensions of the existing model as shown in Fig. 2. Design and operating conditions used for CFD model was based on the demilitarization facility, which is currently being operated to deal with small-sized munitions [16]. The rotary kiln consisted of two inlets, which serve as the entry points of ammunition and hot air. Heat was transferred to the system by the burners located at the air inlet. Flue gases exited the incinerator at the top left part while solid RDX was introduced at the center of the figure. The region in which RDX was introduced was adapted so as to adequately capture the flow physics at the inception of the phase change and chemical reactions. The Eulerian multiphase model was used for gas, liquid, and solid phase and k-ε model was adapted for turbulent gas flow.

The flow physics and solver algorithm were considered in the generation of a good mesh. The less skewed the cells, the more accurate the CFD results and the faster the convergence of the solution [15]. The boundary conditions and physical properties used in this simulation are presented in Tables 1 and 2.

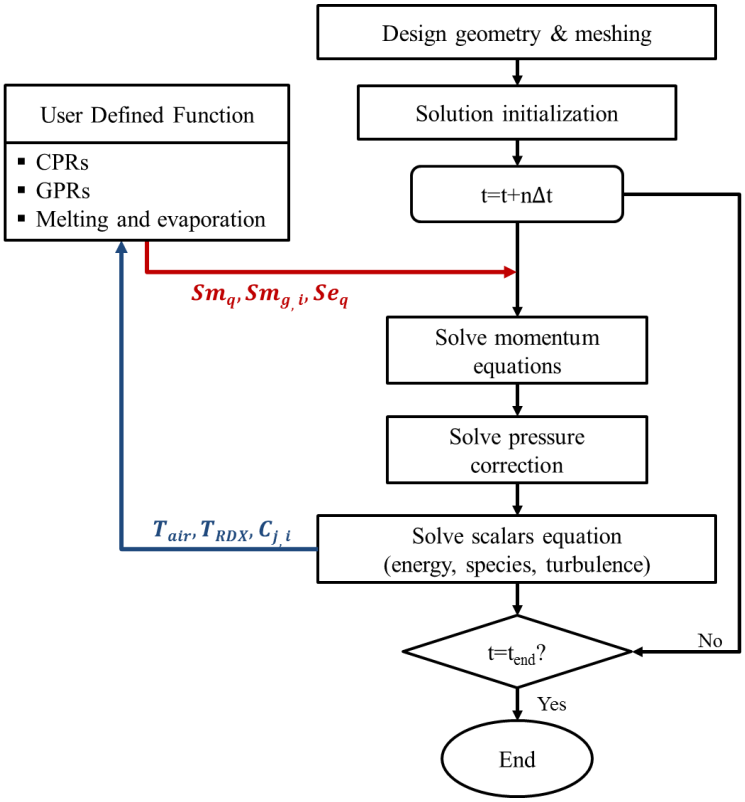

Fig. 1. Schematic diagram for CFD simulation procedure of Eulerian multiphase model.

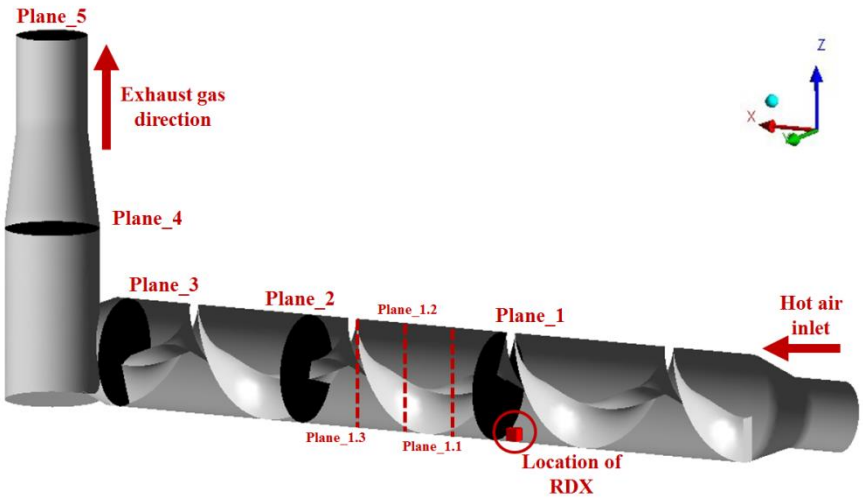

Fig. 2. The structure of the rotary kiln with various axial positions from Plane_1 to Plane_5.

Table 1. Basis for CFD simulation.

Parameter	Description
Primary phase	Gas mixture
Secondary phase	Liquid RDX
Tertiary phase	Solid RDX
Operating temperature	650 K
Initial temperature of RDX	300 K
Initial pressure	1E5 Pa
Inlet air velocity	0.5 m/s
Length of rotary kiln	6 m
Diameter of rotary kiln	1 m

Table 2. Physical properties of RDX [1, 8].

RDX Solid	Value
Density	1820 kg/m^3
Melting temperature	478 K
Melting enthalpy	36000 J/mol
Decomposition temperature	486 K
Ignition temperature	533 K

2.1.1. Mass conservation

For multiphase flows, the continuity equation is solved for the primary phase (gas phase) and secondary phase (the solid RDX and the transitory liquid phases).

$$\frac{\partial}{\partial t}(\alpha_q \rho_q) + \nabla \cdot (\alpha_q \rho_q \vec{v}_q) = \sum_{p=1}^{n} (\dot{m}_{pq} - \dot{m}_{qp}) + Sm_q MW_i \ , \quad Sm_q = \{Sm_s, Sm_l, Sm_g\} \tag{1}$$

$$Sm_s = -Sm_{l,RDX}^{melt} \tag{2}$$

$$Sm_l = Sm_{l,RDX}^{melt} - r_{CPR1} - Sm_{g,RDX}^{evap} \tag{3}$$

$$Sm_g = \sum_{i=1}^{n} Sm_{g,i} \tag{4}$$

$$\frac{\partial}{\partial t}(\rho Y_i) + \nabla \cdot (\rho \vec{v} Y_i) = -\nabla \cdot \vec{J}_i + Sm_{g,i} MW_i \tag{5}$$

$$Sm_{g,i} = Sm_{g,i}^{rx} + Sm_{g,RDX}^{evap} \tag{6}$$

Here, the mass source Sm_q represents the rate at which gases and liquid are generated through evaporation, chemical reaction, and melting condition. The mass source term is further elaborated in Eqs. (9) to (17).

2.1.2. Momentum conservation

The momentum equation solved for each phase within the computational domain is illustrated in Equation 7 as follows.

$$\frac{\partial}{\partial t}(\alpha_q \rho_q \vec{v}_q) + \nabla \cdot (\alpha_q \rho_q \vec{v}_q \vec{v}_q) = -\alpha_q \nabla p + \nabla \cdot \bar{\bar{\tau}}_q + \alpha_q \rho_q \vec{g} + \sum_{p=1}^{n} (\vec{R}_{pq} + \dot{m}_{pq} \vec{v}_{pq} - \dot{m}_{qp} \vec{v}_{qp}) + S_{Fq} \quad (7)$$

2.1.3. Energy conservation

The energy balance includes an accumulation term, axial and radial effective heat conduction term, and convection and energy source terms due to the reactions occurring. The energy equation solved by the CFD tool is also presented in Equation 8.

$$\frac{\partial}{\partial t}(\alpha_q \rho_q h_q) + \nabla \cdot (\alpha_q \rho_q \vec{v}_q h_q) = -\alpha_q \frac{\partial p_q}{\partial t} + \bar{\bar{\tau}}_q : \nabla \vec{v}_q - \nabla \vec{q}_q + \sum_{p=1}^{n} (\vec{Q}_{pq} + \dot{m}_{pq} h_{pq} - \dot{m}_{qp} h_{qp}) + Se_q \quad , \quad (8)$$

$$Se_q = \left\{ Se_s^{ht}, Se_l^{ht}, Se_g^{rx} \right\}$$

The energy source encompasses the heat of reaction and the enthalpy associated with the phase transition of RDX. The heat required for phase change is represented by in Equation 16 while the heat of reaction from CPRs and GPRs is shown in Equation 11.

2.2. Reaction mechanisms

Thermal decomposition of RDX consists of CPRs and GPRs. Solid phase RDX is heated by the hot air and phase change occurs from solid to liquid when the temperature of RDX reaches the melting point(478 K). Mass of liquid RDX decreases by CPR1 and evaporation, and gaseous RDX is consumed through CPR2. Gas components (N_2, N_2O, NO_2, CH_2O, O_2) from CPR1, 2 and inlet air decompose to produce the final gas mixture (NO, CO, CO_2, H_2O) by GPR as illustrated in Fig. 3.

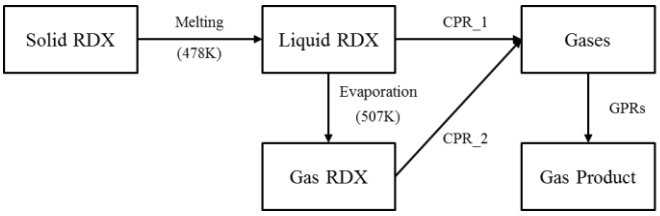

Fig. 3. Mechanism of thermal decomposition of RDX [23].

Considering the number of reactions and the species generated from the detailed chemical kinetics, we resorted to using the global condensed and gas phase reactions presented in Table 3. The corresponding activation energies and frequency factors of reactions are also illustrated in Table 3.

Table 3. CPRs and GPRs of RDX [7].

Reaction type	**Reaction**		
CPR	RDX(liquid,gas) $\longrightarrow$ $1.5N_2+N_2O+NO_2+3CH_2O$		
GPR	$5/7CH_2O+NO_2$ $\longrightarrow$ $NO+2/7CO_2+3/7CO+5/7H_2O$		
Parameter	**A** **[1/s or m^3/mol·s]**	**E** **[J/mol]**	**Heat of reaction** **[J/mol]**
CPR1(liquid)	3.0E18	-173470	330595.140
CPR2(gas)	3.16E15	-173470	424595.140
GPR1(T <970 K)	1.0E9	-79420	192559.074
GPR2(T≧970 K)	1.26E10	-111606	

The mass and heat sources due to thermal decomposition are illustrated in Equations 9-11, where r_{rn} is the reaction rate of CPRs and GPRs. $Sm_{g,i}^{rx}$ is the mass source of gas arising from the CPRs and GPRs, and Se^{rx} is heat of reaction by CPRs and GPRs.

$$r_j = A_j \exp(\frac{-E_j}{RT}) \prod C_{j,i} \tag{9}$$

$$Sm_{g,i}^{rx} = \sum_{j=1}^{n} r_j \xi_{j,i} \tag{10}$$

$$Se_g^{rx} = \sum_{j=1}^{j} r_j \left(\Delta H_r\right)_j \tag{11}$$

2.3. Melting and evaporation

Thermal decomposition of RDX begins with melting. Upon the production of the condensed phase RDX, an array of processes occurs concomitantly. These involve reactions in the condensed phase and evaporation of the liquid RDX which reacts in the gas phase. This results in a consideration of the mass and energy source terms viz: the phase change source term accounting for melting and evaporation as well as the chemical reaction source terms illustrated in the preceding section. These phenomena are modelled with UDF and introduced into the FLUENT solver. The part of the UDF describing phase change is illustrated in Equations 12-17. The overall heat change includes both sensible and latent heats. Heat is continuously transferred to the solid or liquid RDX and phase change occurs when the temperature of RDX is reached at the melting /evaporation points. This phenomenon is implemented in the UDF in the form of an if-else structure. Se_n^{ht} and $Sm_{m,RDX}^{k}$ are the heat and mass sources for the phase change of RDX. When the melting/evaporation temperature of RDX is attained, heat transfer to the surface of RDX for phase change is calculated by Equation 15-16 with the accompanying mass source evaluated by Equation 17 while Equation 12-14 are set to zero at RDX temperatures below the phase change temperatures [24].

If $T_{RDX}^{n} < T_k$ *then*

$$q^k = 0 \tag{12}$$

$$Se_n^{ht} = 0 \tag{13}$$

$$Sm_{m,RDX}^k = 0 \tag{14}$$

Else

$$q^k = h\, A_{n,RDX}\,(T_{air} - T_k) \tag{15}$$

$$Se_n^{ht} = q^k / V_{reactor} \tag{16}$$

$$Sm_{m,RDX}^k = \frac{1}{MW_{RDX}}\left(\frac{Se^{ht}}{H_{latent,k}}\right) \tag{17}$$

$$\left\{\begin{array}{l} Transition\ frome\ solid\ to\ liquid, \\ \quad n = solid(s),\ k = melting(melt),\ m = liquid(l) \\ and\ evaporation\ frome\ liquid\ to\ vapor, \\ \quad n = liquid(l),\ k = evaporation(evap),\ m = gas(g) \end{array}\right\}$$

3. Result and Discussion

The safe operation of rotary kilns for the thermal decomposition of RDX within stipulated environmental limits requires the prevention of hotspots. This is highly linked to the velocity, temperature, and gas composition within the system. An analysis of the variations and effects of these process variables is discussed as follows.

3.1. Velocity

Velocity distribution within the rotary kiln has been monitored from the time of RDX introduction until extinction as shown in Fig. 4. It can be observed that the fluid swirls along with the inner structure of the rotary kiln with the screw. The production of gaseous species as a consequence of thermal decomposition and the volumetric expansion of gases at higher temperatures contribute to the increased gas velocity downstream of the RDX zone. The maximum velocity of gas at the outlet of the rotary kiln has been found to be about 0.98 m/s as illustrated by the velocity vectors of Fig. 4, which is higher than a value of 0.5 m/s at the inlet.

3.2. Temperature profile

The reaction rate of RDX increases exponentially with temperature as indicated by the form of Arrhenius equation representing its reaction kinetics. High explosives such as RDX react at very fast rates with enormous heat release. The aggregate of enthalpies of reactions and the heat from hot air result in a change in the system temperature. Temperature variation within the rotary kiln is observable from the temperature contours shown in Fig. 5. Fig. 5(a) to (d) illustrated time transient temperature profile in the rotary kiln due to the heat of reaction of CPRs and GPRs. After 10s, the increase in temperature locally distributed from 650 K

to 1200 K at plane_1 is primarily due to CPRs with GPRs playing a minor role as can be seen in the production of NO within this time frame as shown in Fig. 10(b). However, with increasing time, Figs. 5(b) to (d), the temperature at the plane_5 rises up to 898 K, which is caused by GPRs. This is deduced from the decrease in CH_2O and increase in NO within this time range as will be shown in Fig. 10.

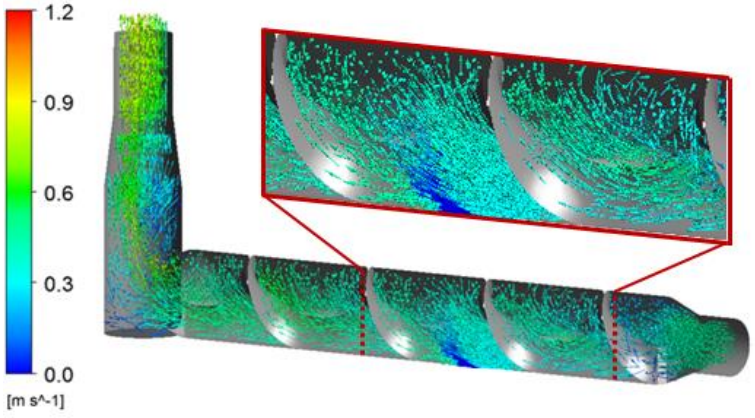

Fig. 4. Simulation result of velocity vector profile in the rotary kiln at 20s.

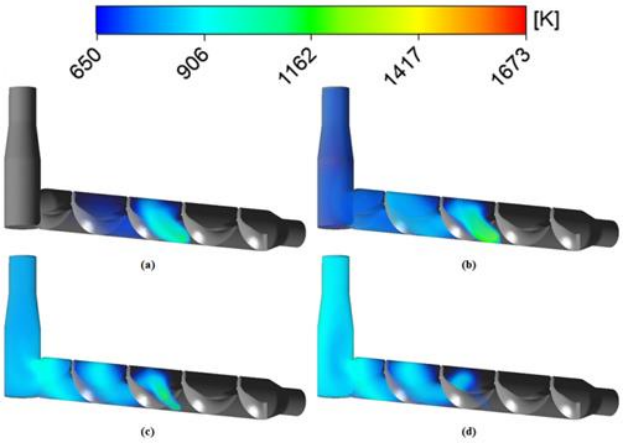

Fig. 5. Model prediction of temperature distribution in the rotary kiln: (a) 10 s, (b) 20 s, (c) 60 s, (d) 80 s.

In order to explicate the variation of temperature within the rotary kiln, planes at vantage points in the 3D geometry as shown in Fig. 2 were used as shown in Fig. 6. Plane_1 is adjacent to the source of RDX and captures the high temperature gases generated by thermal decomposition. Plane_1.1, 1.2, and 1.3 are distributed between plane_1 and 2, and they show the impact of the screw structure, which is occupied by empty space and turned clockwise from plane_1 to 3. Downstream temperature in the rotary kiln decreases and it is quite uniform as shown in planes_2-5 compared with plane_1.The maximum local temperature

due to the decomposition of RDX has been found to be around 1200 K after 20s. This temperature is far higher than the hot air temperature (650 K) used to initiate the reaction and thus the hot air has functions as a coolant in the system. The maximum temperature obtained in this work is less than the flame temperature of RDX (2500 K) as obtained by [25] indicating the suitability of these operating conditions without detonation.

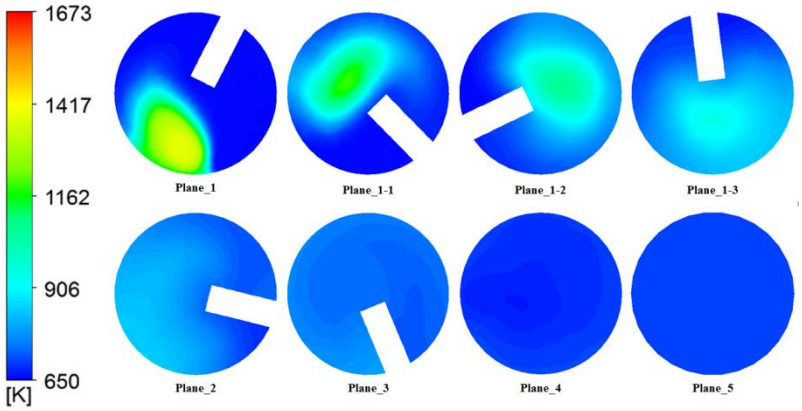

Fig. 6. Temperature distribution along with various axial positions from plane_1 to 5 at 20s (Refer to Fig. 2 for the location of plane_1-5).

3.3. Change of RDX

In the rotary kiln, hot air from the burners provide the impetus required for phase change and thermal decomposition as illustrated by the change in solid volume fraction with temperature and the change in mass of RDX in Fig. 7. This is due to the simultaneous occurrence of CPRs with melting below the vaporization temperature of RDX. Rapid decomposition of RDX occurs under the influence of the surrounding hot air, leading to the consumption of about 68% of RDX in 10s as shown in Fig. 7(a). The decrease in RDX mass proceeds with a slower rate after 10s. Only about 2% of the initial mass of RDX remains within the rotary kiln after 40s as illustrated in Fig. 7.

3.4. Gas composition

Chemical reactions lead to the generation of products which may be highly toxic or environmentally polluting. It is therefore imperative to track the variation of these gaseous products within the rotary kiln. CH_2O, NO_2, N_2O, and N_2 are the primary constituents of the gas phase. Production of CH_2O increases with time with a maximum mole fraction of 0.252 as shown in Fig. 8. It is produced in the vicinity of the solid RDX as captured on plane_1 at 5s, decreasing with time to 0.159 on plane_5 at 21s. The decrease in mole fraction between plane_1 and plane_5 is attributable to the occurrence of GPRs. As a result of the GPRs, NO, CO_2, CO and H_2O are generated. Compared with the mole fraction of CH_2O, the NO generated is relatively lower as shown in the contours of mole fraction in Fig. 9 with its maximum mole fractions of 0.019 and 0.049 in plane_ 1 and 5.

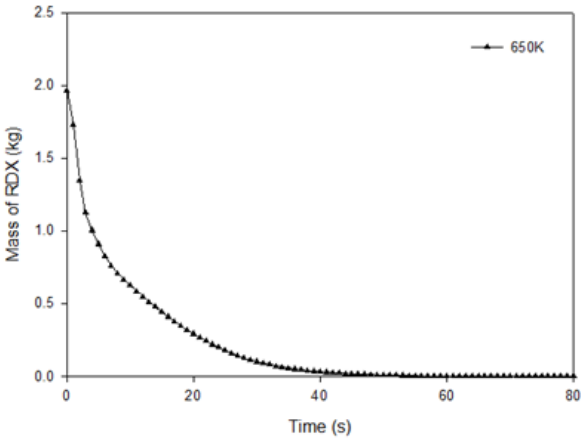

(a) Change in the solid phase RDX by thermal decomposition.

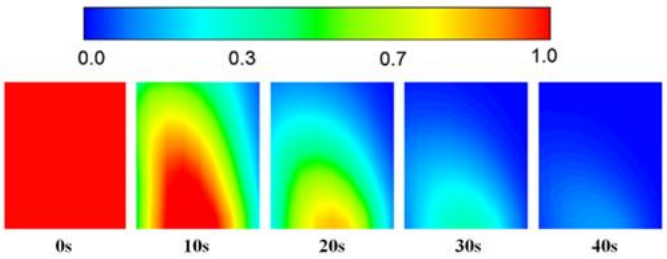

(b) Surface profile of the solid phase RDX volume fraction in the RDX zone.

Fig. 7. Simulation result of mass and volume fraction of solid phase RDX from thermal decomposition.

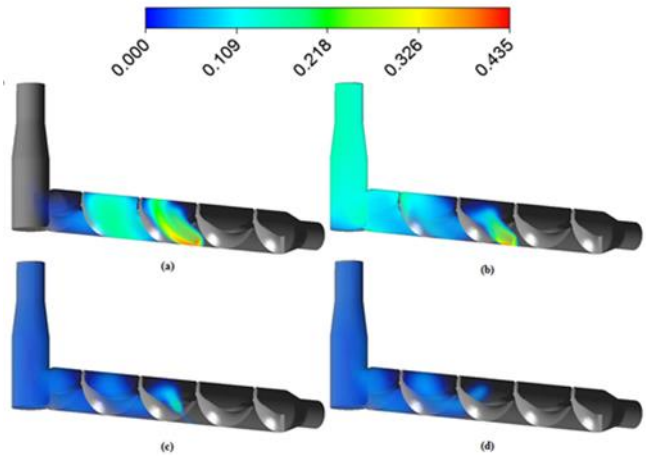

Fig. 8. Transient change in the mole fraction of CH_2O due to CPRs in the rotary kiln: (a) 10 s, (b) 20 s, (c) 60 s, (d) 80 s.

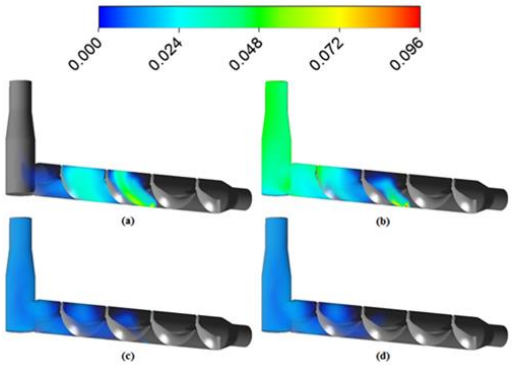

Fig. 9. Transient change in the mole fraction of NO due to GPRs in the rotary kiln: (a) 10 s, (b) 20 s, (c) 60 s, (d) 80 s.

The main components in the gas phase and how they vary with time and position within the rotary kiln are illustrated in Fig. 10. The difference in mole fraction of the 2 compounds (CH_2O, NO) may be analyzed with respect to the stoichiometric coefficients of CPRs and GPRs. CH_2O produced by CPRs are rapidly consumed in the GPRs leading to lower amounts of CH_2O in the vent compared with plane_1. However, at distances further away from RDX source, variations in the amounts of components occur due to the occurrence of GPRs, leading to the increase in the amounts of NO to maximum amounts before decreasing due to the complete consumption of RDX.

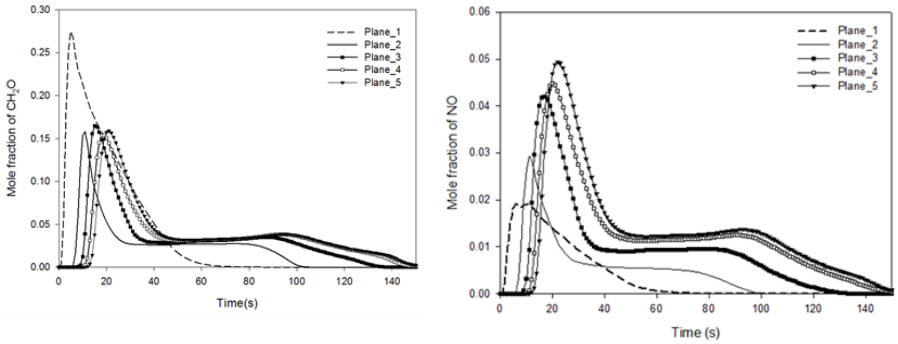

(a) Average mole fraction of CH_2O in the various axial positions from plane_1 to 5.

(b) Average mole fraction of NO in the various axial positions from plane_1 to 5.

Fig. 10. Transient change in the mole fraction from thermal decomposition of RDX (Refer to Fig. 2 for the location of plane_1-5).

4. Conclusions

In this study, CFD simulations were executed to evaluate the dynamic behavior of thermal decomposition in RDX in a commercial scale rotary kiln. Time transient change of velocity and temperature has been examined. In describing thermal decomposition more accurately, phase change such as melting and evaporation was considered and its impact was coded using UDF in FLUENT. 2 CPRs and 2

GPRs were employed in the CFD simulation. The maximum temperatures of exhaust gases were about 898 K, which illustrated safe thermal decomposition without severe ignition. The maximum amounts of CH_2O as well as NO produced in the thermal decomposition process were found to be highly dependent on the temperature of hot air used. From this study, it was concluded that thermal decomposition of RDX can be safely carried out at temperatures with the suggested conditions. Furthermore, thermal decomposition with proper operating conditions led to the prospect of demilitarization of waste explosives in avoiding the possibility of detonation.

Acknowledgements

This research was supported by the Next-generation Converged Energy Material Research Center and Agency for Defense Development.

References

1. Akhavan, J. (2004). *The chemistry of explosives*. Canfield University, Roya; Military college of science, Second edition, Swindon.
2. Kim, H.S. (2006). Basic technologies for the development of high explosives. *Korea Chemical Engineering Research*, 44(5), 435-443.
3. UN Safer Guard, (2011). *International ammunition technical guideline: Demilitarization and destruction of conventional ammunition*. United Nations Headquarters, Fist edition, New York.
4. Wilkinson, J.; and Watt, D. (2006). *Review of demilitarization and disposal techniques for munitions and related materials*. NATO Headquarter, Brussels.
5. Rylott, E.L.; Lorenz, A.; and Bruce, N.C. (2011). Biodegradation and biotransformation of explosives. *Current Opinion in Biotechnology*, 22(3), 434-440.
6. Freedman, D.L.; and Sutherland, K.W. (1998). Biodegradation of hexahydro-1,3,5-trinitro-1,3,5-triazine (RDX) under nitrate-reducing conditions. *Water Science and Technology*, 38(7), 33-40.
7. Ermolin, N.E.; and Zarko, V.E. (1998). Modeling of cyclic-nitramine combustion. *Combustion, Explosion, and Shock Waves*, 34(5), 485-501.
8. Prasad, K.; Yetter, R.A.; and Smooke, M.D. (1997). An eigenvalue method for computing burning rates of RDX propellants. *Combustion Science and Technology*, 124(1-6), 35-82.
9. Zarko, V.E.; and Ermolin N.E. (2001). Investigation of the properties of a kinetic mechanism describing the chemical structure of RDX flames. I. Role of individual reactions and species. *Combustion, Explosion, and Shock Waves*, 37(2), 123-147.
10. Liau, Y.C.; Kim E.S.; and Yang, V. (2001). A comprehensive analysis of laser-induced ignition of RDX monopropellant. *Combustion and Flame*, 126(3), 1680-1698.
11. Long, G.T.; Vyazovkin, S.; Brems, B.A.; and Wight, C.A. (2000). Competitive vaporization and decomposition of liquid RDX. *The Journal of Physical Chemistry B*, 104(11), 2570-2574.

12. Brill, T.B. (1996). *Chemical mechanisms at the burning surface*. Department of Chemistry, University of Delaware, Newark.
13. Schroeder, M.A. (1985). *Critical analysis of nitramine decomposition data: Product distributions from HMX and RDX decomposition*. US Army Ballistic Research Laboratory, Maryland.
14. Gibbs, T.; and Popolato, A. (2014). *LASL explosive property data*. University of California, California.
15. ANSYS, (2014). ANSYS FLUENT: Theory guide. ANSYS Inc., Version 15, USA.
16. Kim, S.H.; Yeom, G.H.; Moon, I.; Chae, J.S.; Kim H.S.; and Min, O. (2014). An analysis of dynamic characteristics of RDX combustion using rigorous modelling. *Clean Technology*, 20(4), 395-405.
17. Ermolin, N.E.; and Zarko, V.E. (2001). Investigation of the properties of a kinetic mechanism describing the chemical structure of RDX flames. II. Construction of reduced kinetic scheme. Combustion. *Explosion, and Shock Waves*, 37(3), 247-254.
18. Liau, Y.C.; and Yang, V. (1995). Analysis of RDX monopropellant combustion with two-phase subsurface reaction. *Journal of Propulsion and Power*, 11(4), 729-739.
19. Beckstead, M.W.; Puduppakkam, K.; Thakre, P.; and Yang, V. (2007). Modeling of combustion and ignition of solid-propellant ingredients. *Progress in Energy and Combustion Science*, 33(6), 497-551.
20. Hossain Khan, M.J.; Hussain,M.A.; and Mujtaba, I.M. (2016). Multiphasic reaction modeling for polypropylene production in a pilot-scale catalytic reactor. *Polymers*, 8(6), 220.
21. Jung, W.; Park, J.; Lee, W.; Lee, J.; Koo, K.; and M. Oh. (2016). Scale-up of a crystallizer for the production of nano-sized energetic materials. *Chemical Engineering & Technology*, 39(7), 1309-1316.
22. Boateng, A.A. (2008). *Rotary kiln: transport phenomena and transport processes*. Elsevier, USA.
23. Kim, S.H.; Nyande, B.W.; Kim, H.S.; Park, J.S.; Lee, W.J.; and Min, O. (2016). Numerical analysis of thermal decomposition for RDX, TNT and composition B. *Journal of Hazardous Material*, 308(5), 120-130.
24. Asante, D.O.; Kim, S.H.; Chae, J.S.; Kim, H.S.; and Min, O. (2015). CFD cook-off simulation and thermal decomposition of confined energetic material. *Propellant, Explosive, Pyrotechnics*, 40(5), 699-705.
25. Kuo, K.K.; and Acharya, R. (2012). *Applications of turbulent and multiphase combustion*. John Wiley & Sons, Inc, New Jersey.